Exploration of BioMat-X

Open Exploration

Open Access Original Article

3D printed hernia mesh implant: a conformability study

Abhishek Barwar[1*], Prateek Kala[1], Rupinder Singh[2], J. Paulo Davim[3]

[1]Department of Mechanical Engineering, BITS Pilani, Pilani 333031, Rajasthan, India

[2]Department of Mechanical Engineering, National Institute of Technical Teachers Training and Research, Chandigarh 160019, India

[3]Department of Mechanical Engineering, University of Aveiro, 3810-193 Aveiro, Portugal

***Correspondence:** Abhishek Barwar, Department of Mechanical Engineering, BITS Pilani, Pilani 333031, Rajasthan, India. barwarabhishek@gmail.com

Academic Editor: Milica Radisic, University of Toronto, Canada

Received: February 27, 2024 **Accepted:** August 29, 2024 **Published:** September 30, 2024

Cite this article: Barwar A, Kala P, Singh R, Davim JP. 3D printed hernia mesh implant: a conformability study. Explor BioMat-X. 2024;1:266–79. https://doi.org/10.37349/ebmx.2024.00019

Abstract

Aim: This study aims to explore the sensing capabilities of polyvinylidene fluoride-hydroxyapatite-chitosan (PVDF-HAP-CS) composite-based hernia mesh implants (of conformal/planar design), followed by in-vitro analysis for better understanding of the bio-stability in the patient's body.

Methods: For analyzing the sensing capabilities, a microstrip patch antenna (MPA)-based implantable sensor [with 17-4 precipitate hardened (PH) stainless steel (SS) (bio-compatible) and Cu alloy (non-biocompatible) materials as conducting plane/patch with PVDF-HAP-CS as dielectric material] has been considered separately in this study. Primarily, in this study, the 3D models of the hernia mesh implant have been designed in the high-frequency structure simulator (HFSS) software, and the sensing behaviour of the same has been recorded.

Results: The HFSS results represent that for the 17-4PH SS-based sensor, resonant frequency (f_r) decreases from 2.3953 to 2.3800 GHz, whereas the gain increases from 0.54 to 4.02 dB with a SAR value of 1.077 W/kg. The f_r for Cu alloy increases up to 30° conformal angle and, after that, starts decreasing, whereas the gain reaches 3.24 dB with a SAR value of 1.238 W/kg. The in-vitro study highlights that both materials (17-4PH SS and Cu alloy) possess a low corrosion rate.

Conclusions: The simulation-based comparison of the biosensors with conducting elements 17-4PH SS and Cu alloy for different conformal angles indicates that the 17-4PH SS shows promising results over Cu in terms of higher gain (up to 4.02 dB) and low SAR value (1.077 W/kg) with the f_r lying in the industry scientific and medical (ISM) band and therefore may be used for implantable sensor applications and possesses the capability to be used as 3D-printed hernia mesh implant. The in-vitro results with the low corrosion rate ≈ of 5.1×10^{-8} mm/year, 17-4PH SS may be a suitable material for the fabrication of hernia mesh implant.

Keywords

Implantable sensor, hernia mesh, conformal design, in-vitro analysis, PVDF composite, HFSS

Introduction

Recently, additive manufacturing (AM) has evolved as one of the most widely explored processes for fabricating bio-medical devices or facilities for medical applications [1]. AM follows a sequential procedure for producing a functional part from a Computer-Aided Design model (CAD) by depositing the material in the form of a layer over the other layer [2]. The ability of AM to produce patient-specific products with complex contours and conformal shapes makes it more popular nowadays [3]. As per ISO ASTM 52900, AM is classified into seven categories depending upon the working principle utilized to join the material successively using the CAD model data. Fused deposition modeling (FDM), among the material extrusion techniques, is one of the most flexible techniques and can process various materials [4]. FDM ensures high dimensional tolerance and improved mechanical strength while processing bio-polymers for producing biomedical implants or scaffolds [5, 6]. Apart from this, among the metal powder-based 3D printing process, direct metal laser sintering (DMLS) offers certain benefits over others, such as acceptable customization capabilities to produce internal structures and external morphology with a range of porosities [7]. DMLS is generally used for fabricating dental and orthopaedic implants utilizing functionally graded materials to achieve elastic strength similar to the bones while minimizing the effect of stress shielding [8, 9]. Various metals and their alloys are used in DMLS printing. Specifically, Ti and stainless steel (SS)-based alloys are the most reported materials for implant fabrication due to their sound mechanical characteristics and corrosion resistance behaviour under in-vivo conditions [10]. The 17-4 precipitate hardened (PH) SS alloy is a suitable biomaterial, offering good mechanical stability and excellent biocompatibility under in-vitro cytotoxicity examination [11, 12].

Diaphragmatic hernia (DH) is one of the most reported maladies among the bovines, and it occurs due to the passage of abdominal viscera into the thoracic cavity [13]. Increased intra-abdominal pressure due to trauma, hardware perforation, or during an advanced stage of pregnancy results in the progressive weakening of the diaphragm and, therefore, leads to the occurrence of thoracoabdominal disorder [14, 15]. Rumenotomy and herniorrhaphy are the most widely used surgical procedures to fix the hernia among bovines [14]. Prosthetic meshes or biological grafts are generally used to overcome the recurrence of DH, as these can provide tension-free repair over the surgical site [16]. A range of bio-materials and their composites were reported in the past for the fabrication of these prosthetic meshes like polyethylene terephthalate, polypropylene (PP), polytetrafluoroethylene (PTFE) and other biological materials also [17–19]. Certain disadvantages of using these synthetic materials are seroma formation, non-comparable tensile strength, adhesions, etc. [20, 21].

PVDF (polyvinylidene fluoride) is a semicrystalline polymer, and due to its piezoelectric nature, it is used extensively for sensing applications [22]. High tensile strength, impact toughness, and biocompatible nature make it suitable for fabricating prosthetic meshes [23]. Reinforcement of filler materials like hydroxyapatite (HAP) and chitosan (CS) can enhance biocompatibility and bioactivity and improve the final component's mechanical strength [24]. Measuring physiological signals produced by any electronic device, such as a transducer or any controlled equipment, is a part of biomedical telemetry for communicating through implantable medical devices [25]. Due to their flexible design, miniaturization, and conformability benefits, implantable patch antennas evolved as a compelling choice for health monitoring applications [26, 27].

The conformal antennas offer impressive properties like reduction in size and capability to work in multiple frequency bands. They are also effective in wearable and implantable applications where round or cylindrical contours are desired [28]. The literature review reveals that much work has been reported on microstrip patch antennas (MPAs) and hernia mesh implants [29–31]. Still, little has been identified on the usage of PVDF-HAP-CS for developing mesh in sensors with a conformal approach to detect the recurrence of DH. In addition, a detailed bibliographic analysis has been performed in this study based on the data extracted through the Web of Science (WOS) database to identify the research gap. For the analysis, keywords like "3D printing", "hernia mesh", "flexibility", "implant", and "conformal" were searched in WOS. As a result, 705 documents appeared (372 were review papers, 263 were research articles, and 640 were journal papers). To further refine the results, a new set of keywords was used, i.e., "biomedical implants",

"flexible" and "in-vitro", and as a result, 108 documents were found. It was observed that with the addition of the keyword "3D printing" in the search string, only 15 papers appeared, indicating that limited work has been reported in the field.

Further, the network diagrams have been constructed using the WOS data to explore the research gaps. VOS viewer (bibliometric tool) was used to build the web diagrams (Figure 1), and the text data obtained from WOS has been processed in VOS viewer. Further, to perform the analysis, the minimum number of occurrences was selected as 6, and based on that, 359 out of 5,092 total terms meet the threshold value. Figure 1a represents the web diagram based on the WOS data obtained after searching for desired keywords. Four clusters based on random term allocation were formed in Figure 1a, represented by different colour codes. Large-size nodes represent the maximum number of interconnections with other nodes and hence represent a current research area that needs to be focused on. Chronic pain, postoperative pain, and hernia repair are among the most highlighted keywords in the network diagram, and they represent the need for a hernia repair solution with enhanced technology to stop the recurrence of DH.

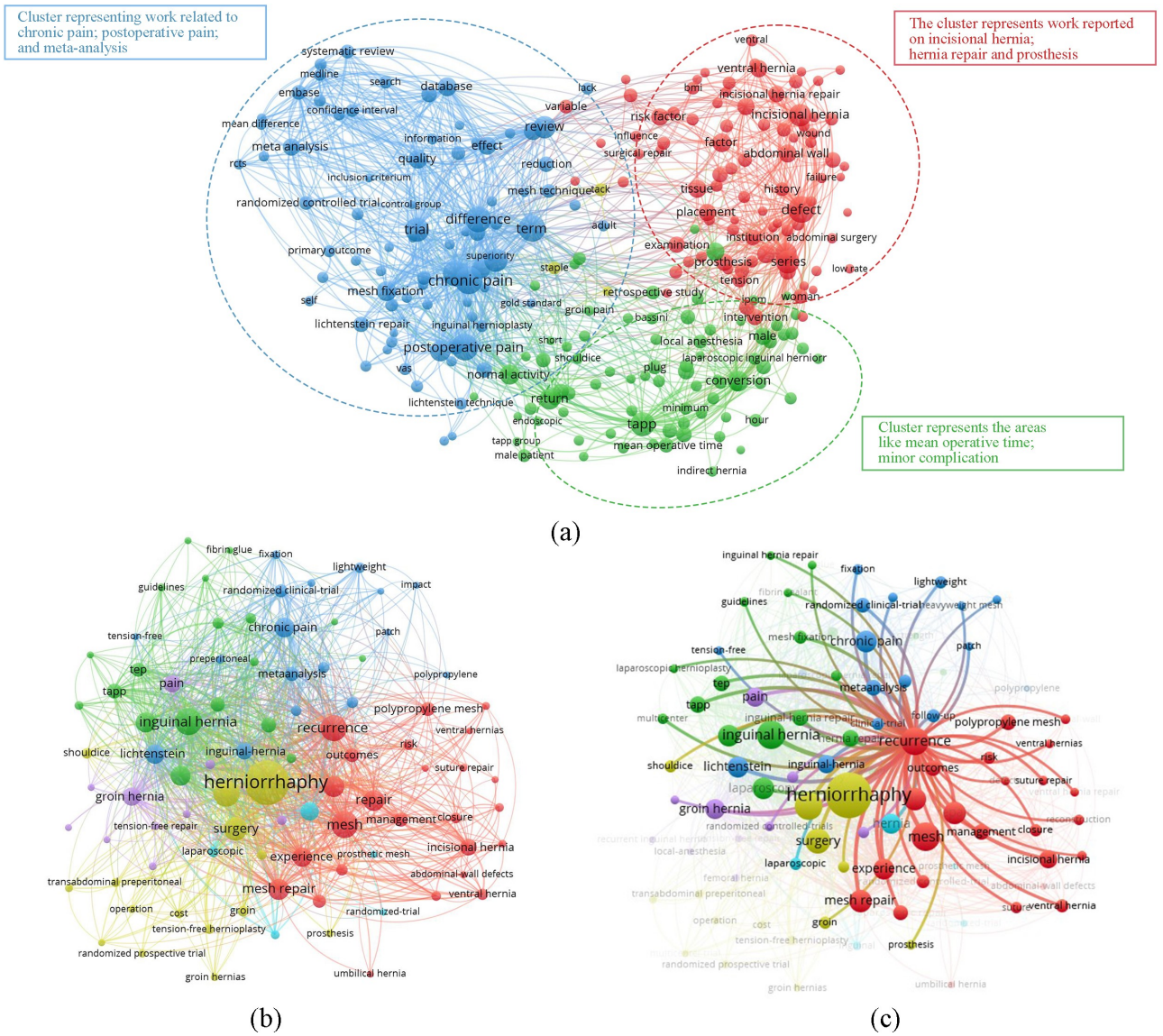

Figure 1. Bibliographic analysis based on the keywords. (a) "3D printing", "hernia mesh", "flexibility", "implant", and "conformal"; (b) "herniorrhaphy", "recurrence", "mesh repair"; (c) co-occurrence analysis based on the keyword "recurrence". Figure 1a contains three broad clusters (i.e., blue, green, and red), other than that, some nodes that appeared in yellow colour are least relevant to the searched keywords as these have very few interconnections with other nodes and small nodes size (representing low weight percentage)

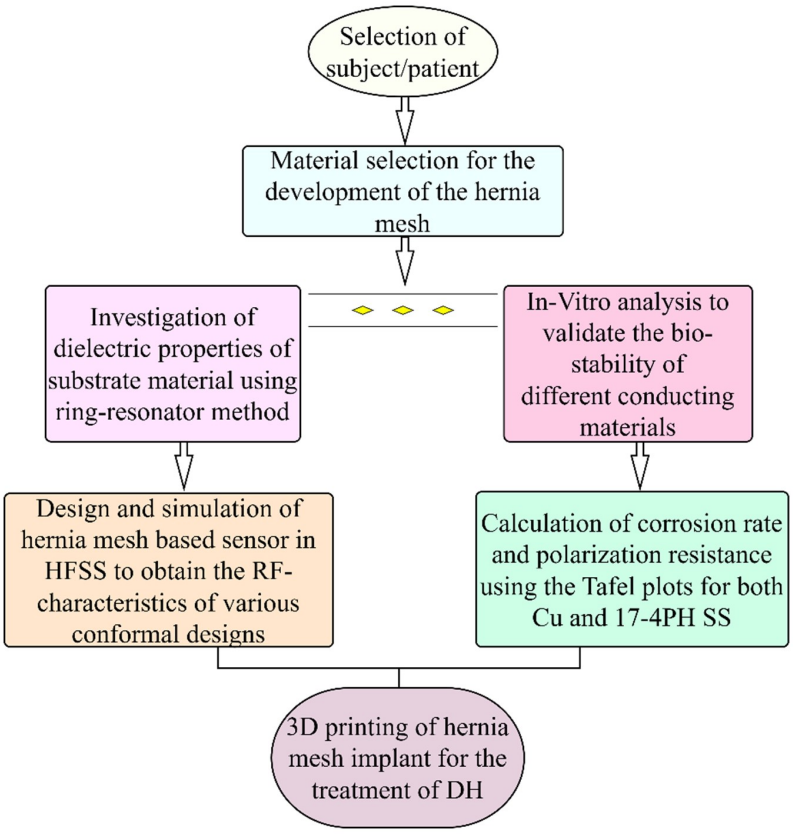

Figure 2. Steps involved in the study. HFSS: high-frequency structure simulator; RF: radio frequency; DH: diaphragmatic hernia

Similarly, Figure 1b represents the network diagram with 5 clusters with different colour codes. In this diagram, nodes with maximum link strength are herniorrhaphy, recurrence, mesh repair, and outcomes. The keyword "recurrence" is highlighted and represented in Figure 1c to perform the co-occurrence analysis further. It was observed that limited materials like PP appeared for fabricating hernia meshes with postoperative complications like recurrence, chronic pain, etc., highlighting the need for material that matches the mechanical properties of the diaphragm and an intelligent solution to monitor a patient's health.

Materials and methods

In this study, 17-4PH SS and Cu were used as conducting materials for analyzing the sensing and conformability behaviour of the mesh in a sensor for the health monitoring of veterinary patients. Usually, Cu, in the form of adhesive tape, is utilized to make the conducting layers of MPA-based sensors. A detailed methodology comprising the steps involved in conducting this study is shown in Figure 2. First, the identification of the nature and severity of the hernia has been ascertained through a medical imaging facility, i.e., X-ray or ultrasonography, and based upon that, the size of the mesh implant has been finalized. Since the hernia mesh implant itself acts as a bio-sensor that works on the principle of MPA therefore, the material selection for the development of hernia mesh was performed based on the mechanical, biocompatible, and dielectric properties of the materials (i.e., PVDF-HAP-CS and 17-4PH SS) [31–33]. This study parallelly investigates the dielectric properties of mesh material (i.e., PVDF-HAP-CS) for designing the conducting materials' bio-sensor and in-vitro properties. Initially, a ring resonator (RR) was designed in the high-frequency structure simulator (HFSS) software to calculate the dielectric parameters [i.e., dielectric constant (ε_r) and loss tangent (tan δ)] of the substrate material while using both Cu and 17-4PH SS as conducting patch and ground planes (for comparison purposes only due to its extensive use in electronic circuits). After the extraction of dielectric parameters, the hernia mesh-based sensors were designed and simulated in the HFSS software to get the radio frequency (RF) behaviour of the sensors [i.e., scattering parameter as reflection coefficient (S_{11}) vs f_r, gain, SAR value, and radiation pattern], and a comparison

study based on the conformal designs and effect on the conducting materials on the performance of sensor has been shown in this work. Simultaneously, an in-vitro analysis of both the conducting materials was performed to analyze the degradability or biostability of the implant inside the body. Linear polarization resistance (R_p), open-circuit potential (OCP), and Tafel analysis have been performed on the conducting materials by making them the working electrode. Finally, based on these analyses, the corrosion rate (CR) for the respective materials has been calculated. Finally, based on the above two comparative analyses, the best suitable settings (conformability and biocompatibility) for manufacturing the hernia mesh implant have been suggested in this study.

In this study, for performing the in-vitro analysis, a metallic component (i.e., 17-4PH SS) having dimensions 50 mm × 20 mm × 4 mm was fabricated through a DMLS 3D printer. For the fabrication of the testing sample, initially, powder processing was performed, which included sieve shaking and preheating of the powder in the hot furnace to remove pre-existing moisture content. Parallelly, the CAD file of the sample was imported into the 3Dxpert software, and build support was provided to the model for easy removal of the part. Previous studies [30] suggest adding inclined wall support results in minimizing residual stresses. Slicing has been done following the adjustment of working parameters, i.e., laser power (LP)—120 W; scanning speed (Sc.S)–1,200 mm/s; and layer thickness (LT)—30 μm.

Medical imaging facility

For making customized biomedical implants or organs, AM has recently evolved as an effective technology capable of fabricating parts with enhanced surface quality utilizing minimum manufacturing time. In this work, the veterinary experts performed an X-ray of the bovine to diagnose the severity of the disease (i.e., DH) and identify the dimensions of the affected area. Figure 3a highlights the bovine under X-ray examination, and the observed data (Figure 3b) highlights the presence of abdominal viscera in the thorax cavity, confirming that the bovine is suffering from DH. While observing closely, the traces of the reticulum (the 2nd compartment of the bovine stomach) have been traced between the 4th and 5th intercostal space and represent the case of thoraco-abdominal disorder. X-ray examinations were conducted as part of routine animal data collection in the X-ray laboratory of GADVASU, Ludhiana, India, and were part of routine non-experimental agricultural practices. These X-ray examinations are not subject to the Breeding of and Experiments on Animals (Control and Supervision) Rules (India). Therefore, ethical approval from the animal experimentation ethics committee is not required.

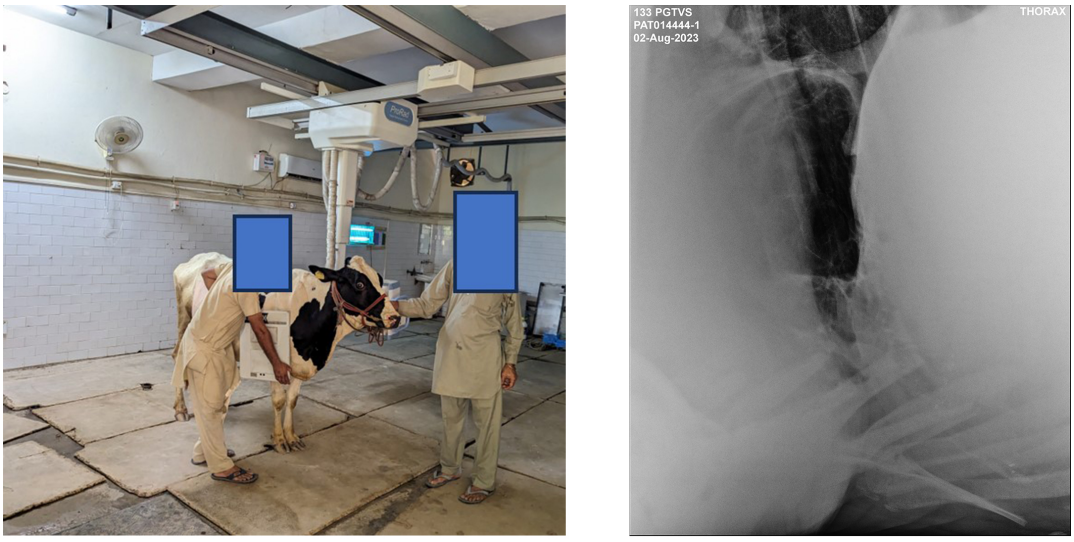

(a) (b)

Figure 3. Diagnosis of DH in the bovine through X-ray examination. (a) The bovine; (b) X-ray examination (image source: X-ray laboratory, GADVASU, Ludhiana, India)

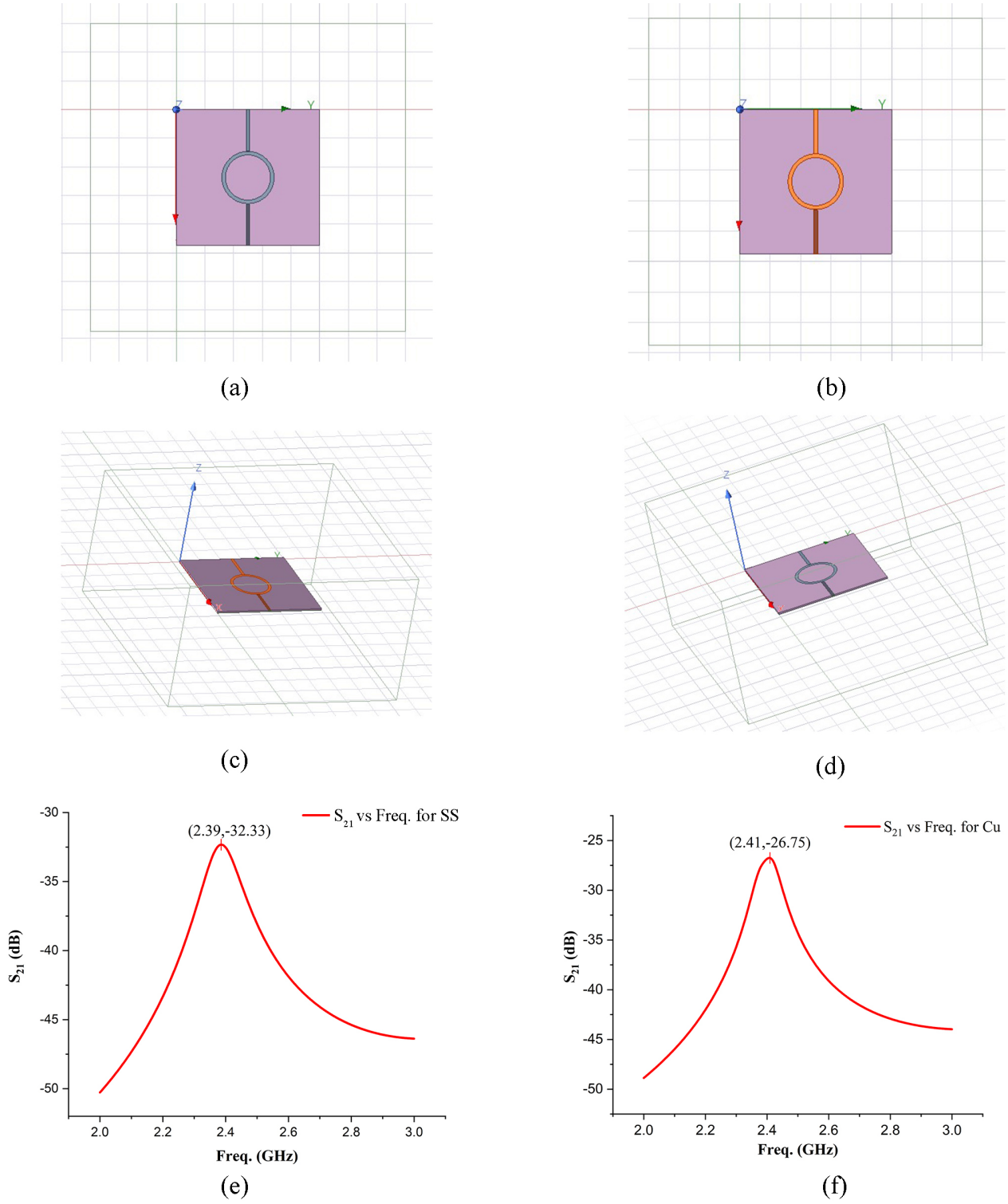

Figure 4. Simulated results of ring resonator test. Ring resonator with 17-4PH SS as conductive material (top view) (a); ring resonator with Cu alloy as conductive material (top view) (b); 3D model of RR with 17-4PH SS (c); 3D model of RR with Cu alloy (d); insertion loss (S_{21}) vs frequency (f_r) with 17-4PH SS (e); S_{21} vs f_r with Cu (f). PH: precipitate hardened; RR: ring resonator; SS: stainless steel

Dielectric characteristics

To identify the dielectric properties of the substrate material, i.e., PVDF-HAP-CS, a standard procedure of ring-resonator (due to low radiation losses) has been followed in this study. The dimensions of the ring and the feed lines have been evaluated using Eq. 1–6 [29], and based on that, an RR has been designed in the HFSS software. Figure 4 represents the designed RR samples with 17-4PH SS and Cu (adhesive tape) as conductive materials for making the ring, feed lines, and ground planes. For analysis of the dielectric parameters, specific input parameters have been required for designing the ring-resonator, i.e., the

theoretical ε_r of substrate material (7.5 for PVDF), thickness of the substrate (0.8 mm), and operating frequency 2.45 GHz for an input impedance of 50 Ω.

$$2\pi R = n\lambda_g \quad \text{Eq. 1}$$

$$\lambda_g = \frac{c}{\sqrt{\varepsilon_{eff}}} \times \frac{1}{f_r} \quad \text{Eq. 2}$$

$$\varepsilon_{eff} = \left[\frac{\varepsilon_r + 1}{2}\right] + \left[\left(\frac{\varepsilon_r - 1}{2}\right)\left(1 + 12\frac{h}{w}\right)^{-0.5}\right] \quad \text{Eq. 3}$$

$$L = \frac{\lambda_g}{4} \quad \text{Eq. 4}$$

$$R_i = R - \frac{w}{2} \quad \text{Eq. 5}$$

$$R_o = R + \frac{w}{2} \quad \text{Eq. 6}$$

R is the mean ring radius, n is the harmonic order for the resonance, λ_g is the guided wavelength of the signal, ε_{eff} is the effective dielectric constant of the substrate material, c is the speed of light, f_r is the resonant frequency, R_i and R_o are the inner and outer radius of the ring, w is the width of the microstrip feed, h is the substrate height, ε_r is the dielectric constant of the substrate material (theoretical value), and L is is the length of the feed line.

It was observed that the RR with 17-4PH SS resonated at 2.387 GHz while possessing the insertion loss of –32.3253 dB, whereas the Cu-based RR resonated at 2.41 GHz with the S_{21} value of –26.75. Further, based on the above behaviour, the dielectric properties of the substrate material have been calculated using Eq. 7 and 8 [29]. Table 1 represents the calculated dielectric properties (ε_r and tan δ) of PVDF-HAP-CS against both conductive materials, i.e., 7.6856, 0.0034 for 17-4PH SS, and 7.4678, 0.0033 for Cu.

$$\varepsilon_r = \frac{(2 \times \varepsilon_{eff} + M - 1)}{M + 1} \quad \text{Eq. 7}$$

$$\tan\delta = \frac{\alpha_d \lambda_o}{27.3}\left(\frac{(\varepsilon_r - 1)\sqrt{\varepsilon_{eff}}}{\varepsilon_r(\varepsilon_{eff} - 1)}\right) \quad \text{Eq. 8}$$

Table 1. Dielectric properties of the PVDF-based composite with different conducting materials

Dielectric properties	Substrate material	
	PVDF-HAP-CS with 17-4PH SS	**PVDF-HAP-CS with Cu tape**
Measured values	S_{21} = –32.33 dB	S_{21} = –26.75 dB
	f_r = 2.39 GHz	f_r = 2.41 GHz
Calculated values	ε_r = 7.6856	ε_r = 7.4678
	tan δ = 0.0034	tan δ = 0.0033

PVDF-HAP-CS input parameters: theoretical ε_r = 7.5; thickness = 0.8 mm. PH: precipitate hardened; PVDF-HAP-CS: polyvinylidene fluoride-hydroxyapatite-chitosan; SS: stainless steel. S_{21} is insertion loss; f_r is frequency; ε_r is the calculated dielectric constant of the substrate material; tan δ is the loss tangent of the material

ε_r is the calculated dielectric constant of the substrate material, ε_{eff} is the effective dielectric constant, M is the function of substrate height and the fringing effect of the microstrip edges, α_d is the attenuation factor of the dielectric, λ_o is the wavelength of the resonance signal in free space, and tan δ is the loss tangent of the material.

Corrosion analysis

An in-vitro analysis was performed against both SS-alloy and Cu (due to their extensive use for sensor fabrications) to analyze the bio-stability of the materials for making implantable biosensors. The analysis used a potentiostat (make: PhadkeSTAT-20, Phadke Instruments, Mumbai, India, with a compatible software EC-Prayog). The experimental setup comprises three electrode unit cells, i.e., the working

electrode (sample to be tested), the counter electrode (graphite), and a reference electrode (a calomel electrode). A simulated body fluid (SBF) (i.e., 2.5 g NaCl in 100 mL of water) has been used to test the samples to mimic the body conditions better. The degradation behaviour of both materials has been observed by performing the Tafel analysis in the SBF.

Results

The conformability study of the hernia mesh implant has been ascertained through the simulation of the biosensors designed in the HFSS software based on the calculated values of the dielectric parameters. Here, in this study, different sensing characteristics have been plotted in the Ansys HFSS for PVDF-HAP-CS substrate using different conducting materials at a time, and the effect of the conformal angle on the sensing characteristics was also examined in this study by varying the conformal angles from 0°, 30°, and 45°. The designed biosensors work on the principle of the MPA and comprise three layers, i.e., a metallic patch, substrate, and a ground plane (metallic). Figures 5 and 6 highlight the sensing behaviour of the designed sensors using 17-4PH SS and Cu as conducting materials, and a comparison of both materials is mentioned in Table 2.

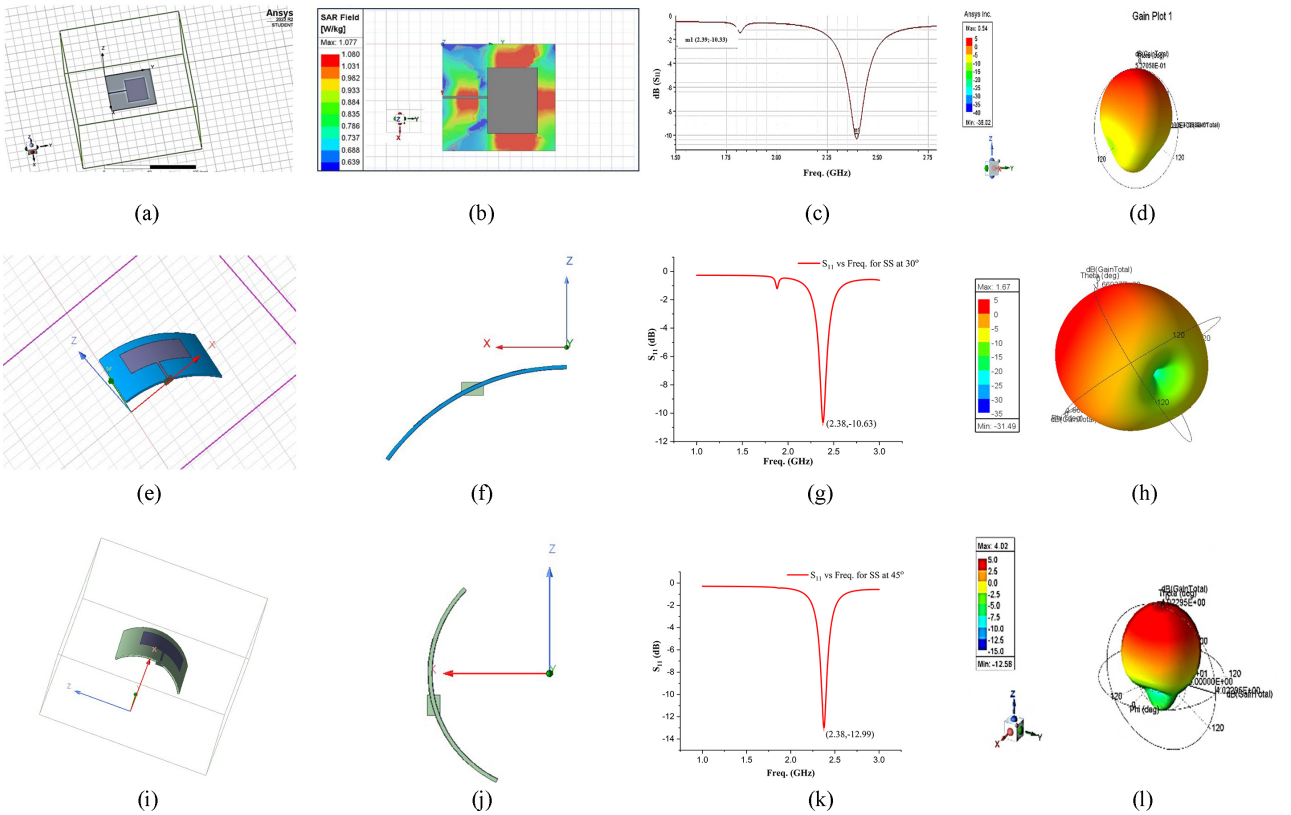

Figure 5. The sensing behaviour of the designed sensors using 17-4PH SS. MPA with 0° conformal angle (a), SAR field at 0° conformal angle (b), S_{11} vs f_r at 0° conformal angle (c), gain value at 0° conformal angle (d); MPA with 30° conformal angle (e), side view of 30° conformal angle (f), S_{11} vs f_r at 30° conformal angle (g), gain value at 30° conformal angle (h); MPA with 45° conformal angle (i), side view of 45° conformal angle (j), S_{11} vs f_r at 45° conformal angle (k), gain value at 45° conformal angle (l). f_r is frequency; S_{11} is reflection coefficient

17-4PH SS-based biosensors

The patch dimensions were calculated using the dielectric value obtained through the RR test to design the MPA-based biosensor. The patch of dimensions 29.38 mm × 22.05 mm has been developed over the substrate. It can radiate (for communication through a remote device) through its surface when an electric signal has been provided. The S_{11} for a frequency range of 1.5 to 3 GHz (ISM band), the gain, and the SAR value have been observed for the designed sensor against different conformal angles. The shift in f_r, SAR, and gain has been examined and compared for both the conducting materials. Figure 5 highlights that the f_r

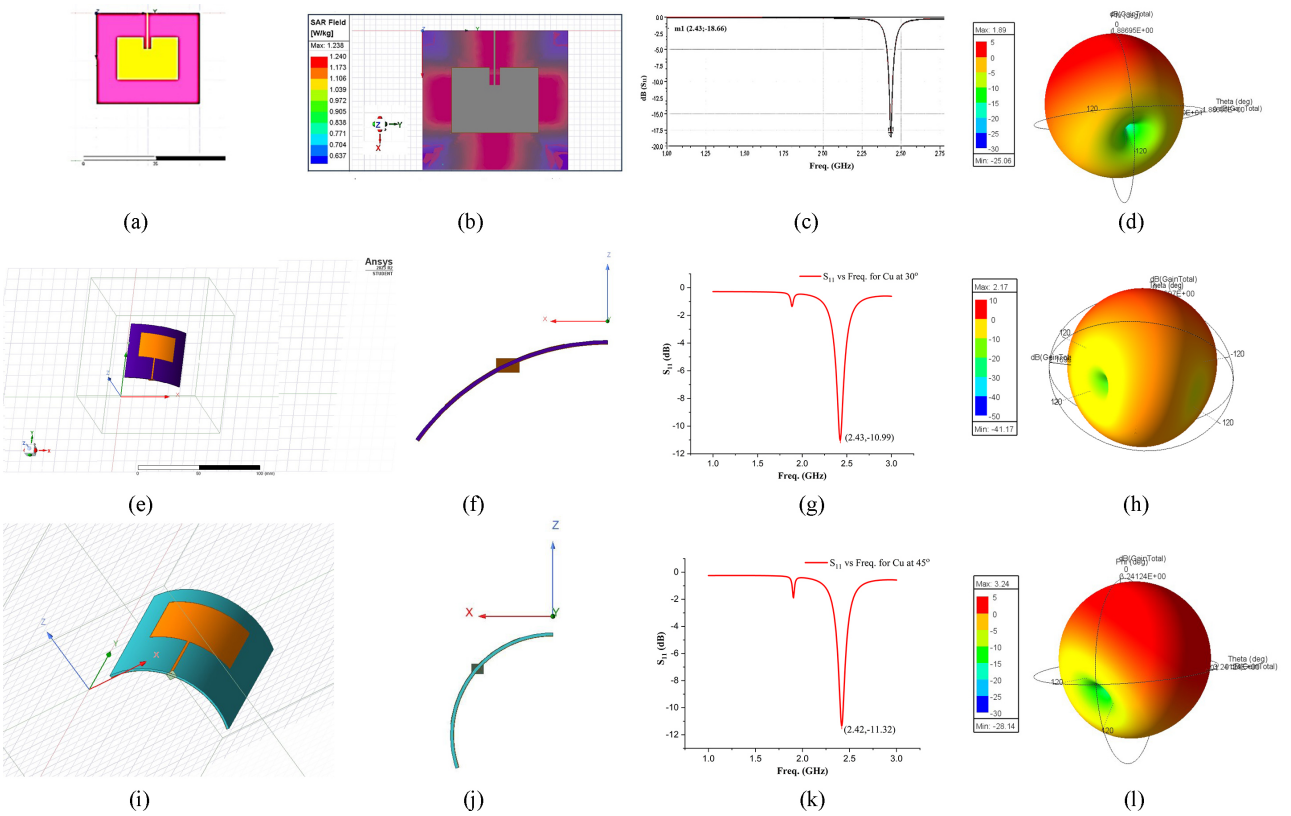

Figure 6. The sensing behaviour of the designed sensors using Cu. MPA with 0° conformal angle (a), SAR field at 0° conformal angle (b), S_{11} vs f_r at 0° conformal angle (c), gain value at 0° conformal angle (d); MPA with 30° conformal angle (e), side view of 30° conformal angle (f), S_{11} vs f_r at 30° conformal angle (g), gain value at 30° conformal angle (h); MPA with 45° conformal angle (i), side view of 45° conformal angle (j), S_{11} vs f_r at 45° conformal angle (k), gain value at 45° conformal angle (l). f_r is frequency; S_{11} is reflection coefficient

Table 2. RF characteristics of the designed sensors at various conformal angles

RF characteristics	Substrate material at various conformal angles					
	PVDF-HAP-CS with 17-4PH SS			PVDF-HAP-CS with Cu adhesive tape		
	0°	30°	45°	0°	30°	45°
Dimensions of parts (in mm)	Ground plane: 47.48 × 50.00 Substrate: 47.48 × 50.00 Patch: 29.38 × 22.05 Feed: 20.00 × 1.05			Ground plane: 47.48 × 50.00 Substrate: 47.48 × 50.00 Patch: 22.36 × 29.75 Feed: 30.00 × 0.70 Slot cut: 6.00 × 3.50		
SAR value (in W/kg)	1.077			1.238		
Gain (in dB)	0.54	1.67	4.02	1.89	2.17	3.24
Scattering parameters (f_r in GHz, S_{11} in dB)	2.39, –10.33	2.38, –10.63	2.38, –12.99	2.43, –18.66	2.43, –10.99	2.42, –11.32

PH: precipitate hardened; PVDF-HAP-CS: polyvinylidene fluoride-hydroxyapatite-chitosan; RF: radio frequency; SS: stainless steel. f_r is frequency; S_{11} is reflection coefficient

shifts in the lower range with the increase in conformal angle, whereas the gain increases with the impressive values and reaches up to 4.02 dB (Figure 5l), representing that the sensor is suitable for communicating through far distances and a SAR value of 1.077 W/kg (Figure 5b) represents the suitability of the material for implantable sensor applications.

Cu based biosensors

Similarly, Cu-based MPA sensors have been designed using HFSS software. Optimization has been performed to achieve the frequency peak in the desired range, and the slots have been provided on the patch. The Cu patch's dimensions were 22.362 mm × 29.754 mm, whereas the slots were 6.00 mm × 3.50 mm per side (Figure 6a). The inferences drawn from the RF characteristics for Cu show that the sensor

with Cu as conductive material possesses more return losses and decreases in frequency value after 30° (Figure 6k), whereas the gain value increases with the increase in curvature angle (Figure 6l). The irregular trend represents the low suitability of the material for such applications.

Table 2 represents the consolidated data of the RF characteristics of the two sensors at different conformal angles. The results indicate that the sensor with 17-4PH SS seems more suitable for implantable conformal sensors for health monitoring of the patients with the ability to transfer the signal to far distance compared to Cu. Also, it possesses low return losses, impressive SAR value, and is biocompatible.

Tafel analysis

The degradation of the materials was analyzed based on the Tafel plots (Figure 7) drawn for both materials. The corrosion current (I_{corr}), as well as the CR, has been evaluated using Eq. 9 and 10 [30]. The R_p of 17-4PH SS is much higher than the Cu, whereas the I_{corr} of Cu (9.00×10^{-7} A) is also higher than the 17-4PH SS (6.56×10^{-7} A). Similarly, the CR of SS-alloy (5.12×10^{-8} mm/year) was observed as lower than the Cu (5.8×10^{-8} mm/year), therefore indicating the marginal difference between the two (Table 3). However, due to the low value of CR, it showcases the suitability of 17-4PH SS for implant applications.

$$I_{Corr} = \frac{1}{R_p} \times \frac{\beta_a \times \beta_c}{2.303\ (\beta_a + \beta_c)} \quad \text{Eq. 9}$$

$$CR = \frac{I_{corr}\ \times EW\ \times K}{\rho \times A} \quad \text{Eq. 10}$$

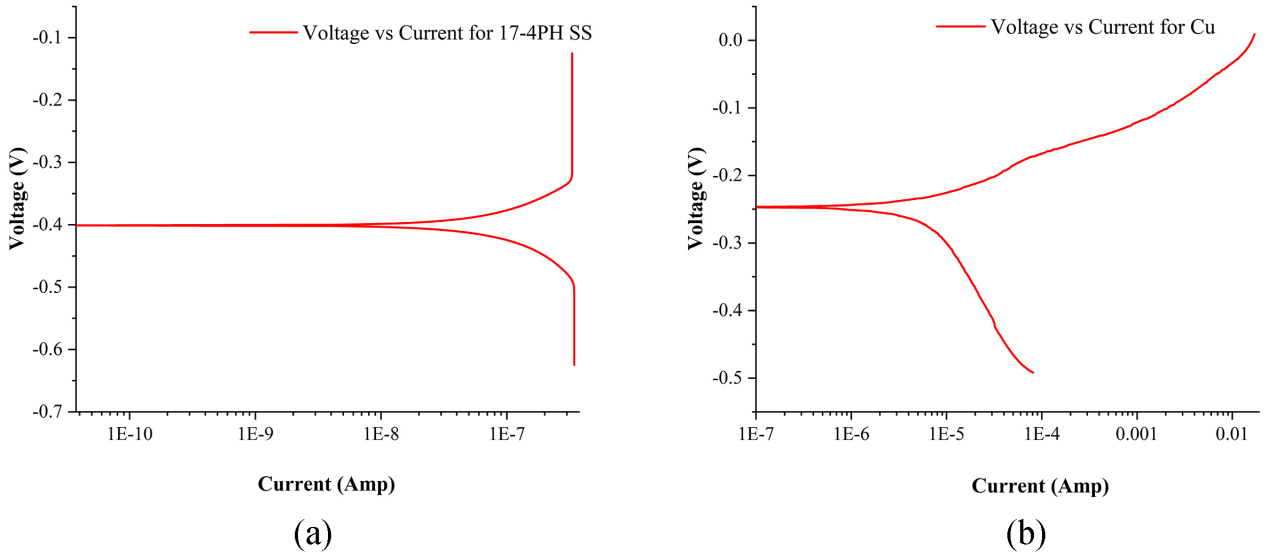

Figure 7. Tafel plots for 17-4PH SS (a) and Cu (b)

Table 3. Comparison table highlighting in-vitro results for both materials

In-vitro results	17-4PH SS	Cu
Linear polarization resistance (R_p) (Ω)	3.05×10^{6}	3.47×10^{4}
Anodic constant (β_a)	0.08404	0.05285
Cathodic constant (β_c)	0.10121	0.19952
Equivalent weight (EW) (g/mol)	27.92	31.80
Density (ρ) (g/cm^3)	7.80	8.96
Exposer area (A) (cm^2)	1.5	1.8
Constant (K) (mm/year)	0.00327	0.00327
Corrosion current (I_{corr}) (A)	6.56×10^{-7}	9.00×10^{-7}
Corrosion rate (CR) (mm/year)	5.12×10^{-8}	5.80×10^{-8}

I_{corr} is the corrosion current, R_p is the polarization resistance, β_a is the anodic constant, β_c is the cathodic constant, EW is the equivalent weight in g/mol, ρ is the material density, A is the exposed cross-sectional area, and K is the constant.

The present study focuses on the conformability of the sensor by analyzing the effect of pressure on the dielectric properties of the sensor mounted on the diaphragm during variable loading conditions as an extension of previously reported work [33]. An in-vivo study is required to ascertain the sensor's performance inside the patient's body. The current work doesn't focus on the self-healing properties of the implant, but it can be explored in further studies to identify the 4D characteristics of the prepared composite. In the future, after obtaining the ethical committee's clinical approval, the implant may be tested inside the body (in vivo) to analyze its compatibility with the surrounding tissues. In future studies, thermal analysis (i.e., differential scanning calorimetry) mimicking autoclaving of the composite may be performed for a range of temperatures to reduce the chances of infection or any complications of the implant inside the body. From the economic and technology transfer perspective, a techno-economic analysis may be performed in further studies to fabricate the sensor.

Discussion

The simulation-based comparison of the biosensors with conducting elements 17-4PH SS and Cu for different conformal angles indicates that the 17-4PH SS shows promising results over Cu in terms of higher gain values (up to 4.02 dB) and low SAR value (1.077 W/kg) with the resonant frequency lying in the ISM band and therefore may be used for implantable sensor applications and may be used as 3D-printed hernia mesh implant. The in-vitro results represent that both Cu and 17-4PH SS possess low values of CR, i.e., 5.80×10^{-8} and 5.12×10^{-8}, respectively. Future studies may be performed on the fabrication of such sensors for smart hernia mesh implants to prevent the recurrence of DH among bovines.

Abbreviations

AM: additive manufacturing

CAD: Computer-Aided Design

CR: corrosion rate

DH: diaphragmatic hernia

DMLS: direct metal laser sintering

HFSS: high-frequency structure simulator

MPA: microstrip patch antenna

PH: precipitate hardened

PVDF-HAP-CS: polyvinylidene fluoride-hydroxyapatite-chitosan

RF: radio frequency

RR: ring resonator

SS: stainless steel

WOS: Web of Science

Declarations

Acknowledgments

The authors acknowledge the research support provided by the National Institute of Technical Teachers Training and Research Chandigarh and Prof. Arun Anand from Guru Angad Dev Veterinary and Animal Sciences University Ludhiana.

Author contributions

AB: Investigations, Writing—original draft, Visualization. PK: Supervisions, Writing—original draft. RS: Conceptualization, Writing—review & editing, Visualization. JPD: Project administration, Writing—review & editing.

Conflicts of interest

Rupinder Singh and J. Paulo Davim who are the Guest Editors of Exploration of BioMat-X had no involvement in the decision-making or the review process of this manuscript. Other authors don't have any conflicts of interest/competing interests.

Ethical approval

X-ray examinations were conducted as part of routine animal data collection in the X-ray laboratory of GADVASU, Ludhiana, India, and were part of routine non-experimental agricultural practices. These X-ray examinations are not subject to the Breeding of and Experiments on Animals (Control and Supervision) Rules (India). Therefore, ethical approval from the animal experimentation ethics committee is not required.

Consent to participate

Informed consent to participate in the study was obtained from relevant participants.

Consent to publication

Informed consent to publication was obtained from relevant participants.

Availability of data and materials

The authors declare that the data can be available on reasonable request.

Funding

The authors thank the Department of Science and Technology, National Institute of Technical Teachers Training and Research for funding under FIST Level-0 [SR/FST/College-/2020/997]. The funders had no role in study design, data collection and analysis, decision to publish, or preparation of the manuscript.

References

1. ISO/ASTM 52900:2021(en) Additive manufacturing — General principles — Fundamentals and vocabulary [Internet]. West Conshohocken (PA): ISO/ASTM; c2021 [cited 2024 Jun 28]. Available from: https://www.iso.org/obp/ui/#iso:std:iso-astm:52900:ed-2:v1:en
2. Kruth JP, Leu MC, Nakagawa T. Progress in additive manufacturing and rapid prototyping. CIRP Ann. 1998;47:525–40. [DOI]
3. Peel S, Eggbeer D, Burton H, Hanson H, Evans PL. Additively manufactured versus conventionally pressed cranioplasty implants: An accuracy comparison. Proc Inst Mech Eng H. 2018;232:949–61. [DOI] [PubMed]
4. Singh R, Barwar A, Kumar R, Kumar V. On mechanically recycled PLA-HAP-CS-based filaments for 3D printing of smart biomedical scaffolds. J Braz Soc Mech Sci Eng. 2022;44:416. [DOI]
5. Yuan L, Ding S, Wen C. Additive manufacturing technology for porous metal implant applications and triple minimal surface structures: A review. Bioact Mater. 2018;4:56–70. [DOI] [PubMed] [PMC]
6. Trenfield SJ, Madla CM, Basit AW, Gaisford S. The shape of things to come: Emerging applications of 3D printing in healthcare. In: Basit A, Gaisford S, editors. 3D printing of pharmaceuticals. Cham: Springer; 2018. pp. 1–19. [DOI]

7. Brunello G, Sivolella S, Meneghello R, Ferroni L, Gardin C, Piattelli A, et al. Powder-based 3D printing for bone tissue engineering. Biotechnol Adv. 2016;34:740–53. [DOI] [PubMed]
8. Calignano F, Manfredi D, Ambrosio EP, Iuliano L, Fino P. Influence of process parameters on surface roughness of aluminum parts produced by DMLS. Int J Adv Manuf Technol. 2013;67:2743–51. [DOI]
9. Traini T, Mangano C, Sammons RL, Mangano F, Macchi A, Piattelli A. Direct laser metal sintering as a new approach to fabrication of an isoelastic functionally graded material for manufacture of porous titanium dental implants. Dent Mater. 2008;24:1525–33. [DOI] [PubMed]
10. Hosseini S, Mirdamadi S, Nemati A. Porous Ti6Al4V scaffolds for dental implants: Microstructure, mechanical, and corrosion behavior. Proc Inst Mech Eng Part L. 2016;230:927–33. [DOI]
11. Brown RN, Sexton BE, Chu TG, Katona TR, Stewart KT, Kyung H, et al. Comparison of stainless steel and titanium alloy orthodontic miniscrew implants: a mechanical and histologic analysis. Am J Orthod Dentofacial Orthop. 2014;145:496–504. [DOI] [PubMed]
12. Mutlu I, Oktay E. Biocompatibility of 17-4 PH stainless steel foam for implant applications. Biomed Mater Eng. 2011;21:223–33. [DOI] [PubMed]
13. Pooniya R, Palsania SK, Saini R, Kumar A, Lal M, Kumar H. Surgico-therapeutic management of diaphragmatic hernia in buffalo: A review of 8 cases. Pharma Innovation J. 2022;SP-11:2118–23.
14. Sharma K, Sangwan V, Kumar A, Singh N, Singh T, Mohindroo J. Diagnosis and surgical outcome of diaphragmatic herniorrhaphy in cows. Large Anim Rev. 2024;30:43–50.
15. Athar H, Mohindroo J, Singh K, Kumar A, Raghunath M. Comparison of radiography and ultrasonography for diagnosis of diaphragmatic hernia in bovines. Vet Med Int. 2010;2010:939870. [DOI] [PubMed] [PMC]
16. Blount AL, Craft RO, Harold KL, Roberts CC. Laparoscopic Repair of a Chronic Iatrogenic Diaphragmatic Hernia. Radiol Case Rep. 2015;4:304. [DOI] [PubMed] [PMC]
17. Valente A, Brereton RJ. Unilateral agenesis of the diaphragm. J Pediatr Surg. 1987;22:848–50. [DOI] [PubMed]
18. Geisler F, Gotlieb A, Fried D. Agenesis of the right diaphragm: repaired with marlex. J Pediatr Surg. 1977;12:587–8. [DOI] [PubMed]
19. Bekdash B, Singh B, Lakhoo K. Recurrent late complications following congenital diaphragmatic hernia repair with prosthetic patches: a case series. J Med Case Rep. 2009;3:7237. [DOI] [PubMed] [PMC]
20. Sugarbaker DJ, Jaklitsch MT, Bueno R, Richards W, Lukanich J, Mentzer SJ, et al. Prevention, early detection, and management of complications after 328 consecutive extrapleural pneumonectomies. J Thorac Cardiovasc Surg. 2004;128:138–46. [DOI] [PubMed]
21. Lee SL, Poulos ND, Greenholz SK. Staged reconstruction of large congenital diaphragmatic defects with synthetic patch followed by reverse latissimus dorsi muscle. J Pediatr Surg. 2002;37:367–70. [DOI] [PubMed]
22. Saxena P, Shukla P. A comprehensive review on fundamental properties and applications of poly (vinylidene fluoride) (PVDF). Adv Compos Hybrid Mater. 2021;4:8–26. [DOI]
23. Lei K, Hsieh Y, Chiu Y, Wu M. The Structure Design of Piezoelectric Poly(vinylidene Fluoride) (PVDF) Polymer-Based Sensor Patch for the Respiration Monitoring under Dynamic Walking Conditions. Sensors (Basel). 2015;15:18801–12. [DOI] [PubMed] [PMC]
24. Ranjan N, Singh R, Ahuja IP, Singh J. Fabrication of PLA-HAp-CS based biocompatible and biodegradable feedstock filament using twin screw extrusion. In: AlMangour B, editor. Additive Manufacturing of Emerging Materials. Cham: Springer; 2019. pp. 325–45. [DOI]
25. Kiourti A, Nikita KS. A review of implantable patch antennas for biomedical telemetry: Challenges and solutions [Wireless Corner]. IEEE Antennas Propag Mag. 2012;54:210–28. [DOI]
26. Soontornpipit P, Furse CM, Chung YC. Design of implantable microstrip antenna for communication with medical implants. IEEE Transactions Microwave Theory Tech. 2004;52:1944–51. [DOI]

27. Kiziltas G, Psychoudakis D, Volakis JL, Kikuchi N. Topology design optimization of dielectric substrates for bandwidth improvement of a patch antenna. IEEE Trans Antennas Propag. 2003;51:2732–43. [DOI]
28. Kiourti A, Nikita KS. Meandered versus spiral novel miniature PIFAs implanted in the human head: Tuning and performance. In: Nikita KS, Lin JC, Fotiadis DI, Arredondo Waldmeyer MT, editors. Proceedings of MobiHealth: International Conference on Wireless Mobile Communication and Healthcare; 2011 Oct 5–7; Kos Island, Greece. Berlin: Springer; 2012. pp. 80–7. [DOI]
29. Singh R, Kumar S, Singh AP, Wei Y. On comparison of recycled LDPE and LDPE–bakelite composite based 3D printed patch antenna. Proc Inst Mech Eng Part L. 2022;236:842–56. [DOI]
30. Boparai KS, Singh R, Kumar A, Pradhan SR, Khan MM. On Tribological and In-vitro Analysis of Meta-Structure-Based 3D Printed Horse Hoof Strap. Natl Acad Sci Lett. 2023;46:117–21. [DOI]
31. Singh S, Singh G, Prakash C, Ramakrishna S, Lamberti L, Pruncu CI. 3D printed biodegradable composites: An insight into mechanical properties of PLA/chitosan scaffold. Polym Test. 2020;89:106722. [DOI]
32. Husain M, Singh R, Pabla BS. A review on 3D printing of partially absorbable implants. J Inst Eng (India) Series C. 2023;104:1113–32. [DOI]
33. Singh R, Singh G, Anand A. On 3D printed intelligent diaphragmatic hernia sensor. Rapid Prototyping J. 2024;30:323–37. [DOI]